

# Grain boundaries exhibit the dynamics of glass-forming liquids

Hao Zhang<sup>a</sup>, David J. Srolovitz<sup>b</sup>, Jack F. Douglas<sup>c,1</sup>, and James A. Warren<sup>d</sup>

<sup>a</sup>Department of Chemical and Materials Engineering, University of Alberta, Edmonton, AB, Canada T6G 2V4; <sup>b</sup>Department of Physics, Yeshiva College, Yeshiva University, New York, NY 10033; and <sup>c</sup>Polymers Division and <sup>d</sup>Metallurgy Division, National Institute of Standards and Technology, Gaithersburg, MD 20899

Edited by Johanna M. H. Levelt Sengers, National Institute of Standards and Technology, Gaithersburg, MD, and approved March 24, 2009 (received for review January 14, 2009)

Polycrystalline materials are composites of crystalline particles or “grains” separated by thin “amorphous” grain boundaries (GBs). Although GBs have been exhaustively investigated at low temperatures, at which these regions are relatively ordered, much less is known about them at higher temperatures, where they exhibit significant mobility and structural disorder and characterization methods are limited. The time and spatial scales accessible to molecular dynamics (MD) simulation are appropriate for investigating the dynamical and structural properties of GBs at elevated temperatures, and we exploit MD to explore basic aspects of GB dynamics as a function of temperature. It has long been hypothesized that GBs have features in common with glass-forming liquids based on the processing characteristics of polycrystalline materials. We find remarkable support for this suggestion, as evidenced by string-like collective atomic motion and transient caging of atomic motion, and a non-Arrhenius GB mobility describing the average rate of large-scale GB displacement.

glass formation | grain-boundary mobility | molecular dynamics | polycrystalline materials | string-like collective motion

Most technologically important materials are polycrystalline in nature (1), and it is appreciated that the grain boundaries (GBs) of these materials, the interfacial region separating the crystal grains (see Fig. 1A), significantly influence the properties of this broad class of materials (2). In particular, the dynamical properties of GBs, such as the GB mobility ( $M$ ), play an important role in the plastic deformation and evolution of microstructure during material processing and service (3).<sup>†</sup>

The atomic organization in the GBs represents a compromise between the ordering effects of adjacent grains, and “packing frustration” [or reduced packing efficiency (6)] is also characteristic of glass-forming (GF) fluids, in which particle ordering is likewise limited in range (7). This simple observation leads us to expect similarities between the dynamics of GBs and GF fluids, and below we provide evidence for this relationship. By implication, GB migration should then be sensitive to impurities, geometrical confinement, and applied stresses—basically any factor that affects particle-packing efficiency (8–10). To illustrate this point and test our perspective of GB dynamics, we quantitatively interpret differences in the effect of large tensile and compressive deformations on  $M$  in terms of measures of cooperative atomic motion drawn from the physics of GF fluids.

Nearly 100 years ago, Rosenhain and Ewen (11) suggested that metal grains in cast iron were “cemented” together by a thin layer of “amorphous” (i.e., noncrystalline) material “identical with or at least closely analogous to the condition of a greatly undercooled liquid.” Although this conceptual model was able to rationalize processing characteristics of ferritic materials (11), it was not possible to validate it at the time through direct observation or simulation. Sixty years later, Ashby (12) “simulated” GB dynamics by using a model system of layers of macroscopic bubbles (“bubble rafts”); he also suggested similarities between GBs and GF liquids. Again, the inability to test this hypothesis on physically realistic GBs limited its acceptance.

Recent molecular dynamics (MD) simulations of polycrystalline metals and silicon by Wolf and coworkers (13, 14) suggest that the disordered structure within GBs can be well described by atomic radial distribution functions characteristic of GF liquids.

Here we directly address what, if any, characteristics GBs share with GF liquids by performing a series of MD simulations on the migration of model GBs at elevated temperatures ( $T$ ) and by comparing the GB MD and GB mobility  $M(T)$  to the MD and large-scale structural relaxation of GF liquids. In Section II we describe GB geometry and our GB model, quantify cooperative atomic motion within the GBs by using measures applied before to GF liquids, compare the  $T$  dependence of  $M(T)$  to the transport properties (e.g., viscosity) of GF liquids, and then determine the characteristic temperatures of GB fluids that define the broad transition in the GB mobility and which have their counterparts in GF liquids. Further comparison of these transitions is included in *SI* to more precisely identify the type of GF liquids that most resemble our simulated GB fluid dynamics. We also illustrate the value of this perspective of polycrystalline materials by applying it to explain changes in  $M(T)$  arising from the form of applied stress (e.g., tensile versus compressive deformation) to which the polycrystalline material is subjected.

## Results

**I. Cooperative GB Atomic Motion and GB Mobility. GB geometry and model.** The crystallography of GB can be minimally specified by five variables: three parameters to specify the relative orientation of one grain with respect to the other and two to indicate the GB inclination (3) (note the distinct orientations of grains indicated in Fig. 1B); a “misorientation angle” describes a rotation of one grain that will cause it to coincide in orientation with the other). Although these variables characterize the basic GB crystallography, they do not fully specify GB atomic structure. GB structure has been variously described in terms of dislocations (15), “structural units” (16), “coincidence site lattices” (CSLs) (3), etc. All of these descriptions of GB structure have their limitations at elevated  $T$ , at which the GBs exhibit appreciable disorder.

Because the geometrical parameters of the CSL provide a prevalent method for GB characterization, we describe aspects of this classification scheme required for our discussion below. For certain misorientation angles between adjacent crystals, a

Author contributions: D.J.S., J.F.D., and J.A.W. designed research; H.Z. and J.F.D. performed research; H.Z. and J.F.D. analyzed data; H.Z. performed molecular dynamics simulations; and J.F.D. wrote the paper.

The authors declare no conflict of interest.

This article is a PNAS Direct Submission.

<sup>1</sup>To whom correspondence should be addressed. E-mail: jack.douglas@nist.gov

<sup>†</sup>In inorganic crystalline materials, the GBs are often as wide as several nanometers (in metals the GB widths are more typically in the 0.2- to 1-nm range). When the grain size is on the nanoscale, the fraction of the material in these GB regions becomes appreciable [in excess of 10% for polycrystalline materials with a grain size of 10 nm (4)], and the GBs can then come to dominate material properties (5).

This article contains supporting information online at [www.pnas.org/cgi/content/full/0900227106/DCSupplemental](http://www.pnas.org/cgi/content/full/0900227106/DCSupplemental).

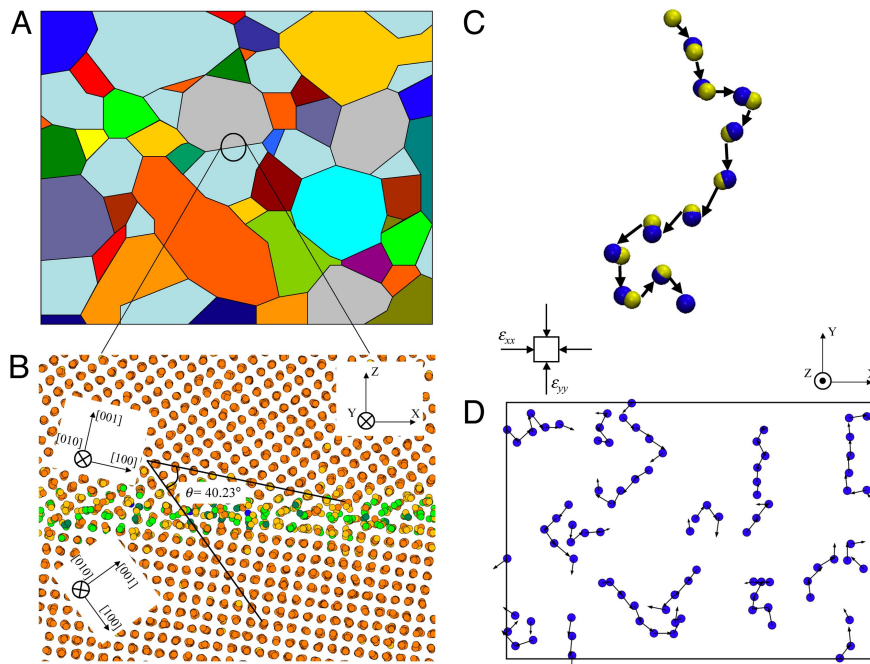


**Fig. 1.** Illustration of string-like cooperative atomic motion within a GB. (A) Schematic microstructure of polycrystalline metal. Different colors indicate the individual grains having different orientations, and the black line segments represent GBs. (B) Equilibrium boundary structure projected onto the  $x$ - $z$  plane for a  $\theta = 40.23^\circ$  [010] general tilt boundary at  $T = 900$  K ( $x$ ,  $y$ , and  $z$  axes are lab-fixed Cartesian coordinates, whereas [100], [010], and [001] refer to crystallographic axes). Upper and lower grains rotate relatively to each other by  $40.23^\circ$  along the common tilt axis [010]. The misorientation angle  $\theta = 40.23^\circ$  does not correspond to a special  $\Sigma$  value [ $\Sigma$  refers to the ratio of the volume of the coincidence site lattice (CSL) to the volume of crystal lattice]. The atoms are colored according to their coordination numbers  $q$  (orange,  $q = 12$ ; others,  $q < 12$ ). The simulation cell was chosen to have the GB plane normal to the  $z$  axis. (C) Representative string within GB plane. Yellow and blue spheres represent the atoms at an initial time  $t = 0$  and a later time,  $t^*$ . (D) Snapshot of string-like cooperative motion within the GB region at  $T = 900$  K at  $\Delta t = t^*$ . The rectangular box illustrates the simulation cell in the  $x$ - $y$  plane. Biaxial strain  $\epsilon_{xx}$  and  $\epsilon_{yy}$  are applied to  $x$ - $y$  plane to induce driving force that arises from the elastic energy difference between two grains, as shown in the diagram above the box.

common superlattice can be defined if the adjacent crystal lattices are formally allowed to interpenetrate each other. This lattice is called a CSL (3), and the corresponding GB is characterized by a “coincidence number”  $\Sigma$ , the ratio of the volumes of the CSL and individual grain lattice cells. For most misorientation angles, there is no CSL, but there is a countable infinity of misorientation angles for which the CSL exists (just a few of these being important in applications), and these GBs are termed “special” or “ $\Sigma$ ” type. On the other hand, in the common case where the GBs are more disordered so that the CSLs are not defined, the GBs are termed “general” or “non- $\Sigma$ ” type. Low  $\Sigma$  value GBs have relatively lower GB energies (3), and materials having a high density of GBs with this symmetric structure give rise to enhanced corrosion resistance and other desirable material properties. However, most materials involve “random” GBs having a broad population of  $\Sigma$  and non- $\Sigma$  GBs that can be altered by changing the annealing history. For generality, we thus investigate both of these basic GB types. Visualizations of  $\Sigma$  and non- $\Sigma$  GBs, which are helpful in developing an intuition for these structures, are given in ref. 17.

Fig. 1B shows a representative non- $\Sigma$  GB having a misorientation angle of  $\theta = 40.23^\circ$  and the coordinate system defining this structure and to which we refer below. The system actually simulated comprises only two crystal grains and the interfacial region between them, a “bicrystal.” The temperature  $T/T_m$  range considered ranges from 0.48 to 0.86, where the reduced  $T$  is defined in terms of the bulk Ni melting temperature,  $T_m = 1,624$  K (18) and where  $T$  is controlled with a Hoover–Holian thermostat (19). An embedded-atom potential (20) describes interactions between the 22,630 Ni atoms in our simulation.

Compressive stresses were applied to the bicrystal (constant stress arises from the application of constant strain along the  $x$

and  $y$  directions, as illustrated in Fig. 1B, where  $x$ ,  $y$ , and  $z$  axes define laboratory coordinates and [100], [010], and [001] define crystallographic axes), giving rise to a change in the elastic free energy of each grain (the crystals are elastically anisotropic) and a thermodynamic driving force for GB displacement. Computation details were described in our previous articles (21, 22).

**Cooperative particle motion within the GB.** Cooperative particle dynamics is one of the most characteristic features of the dynamics of GF fluids. In particular, both atomistic simulations and experiments on colloidal and granular fluids demonstrate that this cooperative motion takes the form of string-like motion (23–26). To examine whether a similar dynamics occurs in the GB regions of polycrystalline materials, we apply methods originally developed to identify this type of motion in GF liquids (23) to our MD simulations of GB atomic dynamics. As a first step in identifying the collective particle motion, we identify the “mobile” atoms in our system (i.e., those that move a distance in a time  $\Delta t$  that is larger than the typical amplitude of an atomic vibration but smaller than the second nearest-neighbor atomic distance). Because there are no defects in either crystal, the average displacement of the atoms within the grains after any  $\Delta t$  is within the scale of the mean vibrational amplitude. Therefore, the identified mobile atoms within  $\Delta t$  are all located within GB region. Next, mobile atoms  $i$  and  $j$  are considered to be within a displacement string if they remain near one another as they move (9, 18, 23) (see Fig. 1C). We indeed find “strings” in our GB dynamics simulations as in GF liquids and provide some characterization of these structures below to determine how their geometry compares to their counterparts in GF fluids. In particular, the average “string length,”

$$\bar{n}(\Delta t) = \sum_{n=2}^{\infty} nP(n, \Delta t). \quad [1]$$

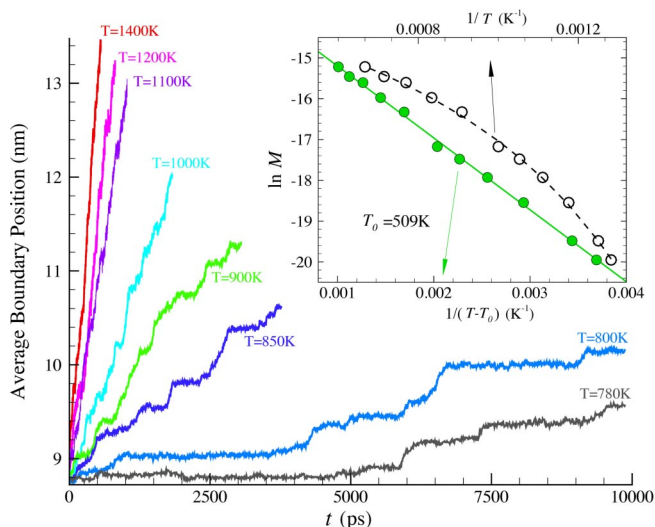


**Fig. 2.** Temporal evolution of the average boundary position at eight different temperatures. (*Inset*) Logarithm of the boundary mobility as a function of  $T$  [open circles versus  $1/T$  (top axis) compare the data to an Arrhenius relationship, whereas the filled circles compare to the VF equation (bottom axis)]. The nonlinearity of the Arrhenius plot indicates that this relationship does not apply to GB mobility data.

provides a natural measure of the scale of cooperative particle motion in strongly interacting liquids where  $P(n, \Delta t)$  is the probability of finding a string of length  $n$  a time interval  $\Delta t$ . Previous work (8, 22) has established that the average length of these strings in GF liquids grows after cooling, along with the effective activation energy for structural relaxation. This finding accords with the Adams–Gibbs theory of relaxation in GF liquids (27), in which the strings are identified (23) with the vaguely defined “cooperatively rearranging regions” of the Adams–Gibbs theory. Strings are thus of practical interest, because they are correlated with the relative strength of the temperature dependence of transport properties (see below), perhaps the most important property of GF fluids.

**Similarity of GB mobility to transport properties of GF liquids.** The GB mobility is defined by the rate of displacement of the GB after the application of a stress to the polycrystalline material so this motion occurs in a direction orthogonal to the plane of the GB in which collective atomic motions primarily occur. Fig. 2 shows the displacement of the GB position as a function of  $t$  for eight representative  $T$  values. Because the structure of GBs is more disordered than that of the crystal grains, the coordination number for most atoms within GB region is normally reduced. On the basis of this observation, the mean GB position can be calculated by averaging the positions of those atoms having this reduced coordination number (see Fig. 1*B* legend). The boundary velocity  $v$  was simply obtained from the average slope of the boundary position versus  $t$ , where final displacements from 1 to 5 nm were considered, depending on  $T$ .

In the classical theory of GB migration (28), the temperature dependence of the GB mobility (ratio of the velocity  $v$  to the driving force  $\Delta p$ ) obeys an Arrhenius temperature dependence [i.e.,  $M = M_0 \exp\{-Q/(k_B T)\}$ ], where  $M_0$  is a constant and  $Q$  is the activation energy for boundary migration. Fig. 2 *Inset* (open circles) shows that this expectation is not satisfied. Instead, if we fit the GB mobility data to the Vogel–Fulcher (VF) equation (29),

$$M = M_{VF} \exp\left(-\frac{Q_{VF}}{k_B(T - T_0)}\right), \quad [2]$$

where  $M_{VF}$ ,  $Q_{VF}$ , and  $T_0$  are material-specific constants, then the fit becomes significantly better. A strong temperature depen-

dence of large-scale transport properties is a characteristic, even defining property, of GF liquids, and the VF equation (Eq. 2) phenomenologically describes structural relaxation and diffusion at low temperatures in an astounding number of GF materials at temperatures higher than the glass transition temperature,  $T_g$ . Eq. 2 does not apply below  $T_g$ , at which an Arrhenius temperature dependence of relaxation is again normally recovered. Because  $T_g$  is generally well above the temperature  $T_0$  at which the rate of molecular diffusion formally vanishes in the VF mobility relation (see Eq. 2), the extrapolation temperature (30)  $T_0$  cannot be literally identified with a condition of vanishing mobility. The same situation is true for the GB mobility,  $M(T)$ , so that  $T_0$  only serves to characterize the strength of the non-Arrhenius temperature dependence of the mobility over a restricted temperature range above  $T_g$ .

A best fit of the data in Fig. 2 to Eq. 2 yields the characteristic temperature,  $T_0 = (509 \pm 18)$  K (error estimate is based on a 95% confidence interval throughout this article), and below we compare the ratio,  $D \equiv Q_{VF}/k_B T_0$ , the “fragility parameter” in GF liquids, for our GB dynamics to  $D$  for appropriate classes of GF fluids. We conclude that the temperature dependence of the GB mobility obeys the same phenomenological relationship as relaxation in GF liquids, providing some support for the physical picture of polycrystalline materials described in our introduction.

We tested the physical sensibility of  $T_0$  in relation to GF fluids by comparing this quantity to the melting temperature  $T_m$ . For metallic glasses, the ratio of the melting (eutectic) temperature to  $T_0$  has been estimated to be  $T_m/T_0 \approx 2.8$  (*SI Text* and Table S1), which is reasonably close to the corresponding ratio  $1624/509$  K = 3.2 that we found for GB migration. We conclude that the magnitude of  $T_0$  that we estimated is quite reasonable in comparison to the phenomenology of GF fluids. Next, we will consider the commonality between the MD of GB motion and GF liquids at a molecular scale.

**Cooperative molecular motion in GB and GF liquids.** As discussed above, string-like cooperative atomic motion is prevalent in all GF liquids examined to date [including water, polymer fluids, metallic GF liquids, concentrated colloidal suspensions, and even strongly driven granular fluids (8, 23, 26, 31, 32)]. It is apparently a universal property of the dynamics of strongly interacting fluids, where a strong reduction in the particle mobility and an enormous change in the rate of structural relaxation are found in association with the growth of string-like correlated motion after approaching the glass transition. We next examine the nature of the atomic motion occurring in GB migration to determine whether it follows this general pattern of “frustrated fluid” dynamics. Fig. 1*C* shows a typical displacement string in our simulation appearing in the plane of the GB region. The initial atom positions are shown in yellow ( $t = 0$ ), and their positions at a later time  $\Delta t$  are shown in blue (displacements are shown by using arrows; see Fig. 2 *C* and *D*). This string-like atomic motion in the GB region occurs predominantly along a direction parallel to the tilt axis (see Fig. 1*D*) but in a direction orthogonal to the ultimate direction of GB displacement.

Atomistic simulations of GF liquids suggest that the distribution of string lengths  $P(n)$  is an approximately exponential function of  $n$ ,

$$P(n) \sim \exp(-n/\langle n \rangle). \quad [3]$$

Fig. 3 shows the distribution of string lengths at  $\Delta t = t^*$ , where the string length  $n(\Delta t)$  exhibits a maximum during GB migration [time dependence of  $n(\Delta t)$  not shown; see refs 22–24]. Interestingly, the distributions of  $n$  in GF liquids and in the GBs are essentially the same (10), and even the magnitude of  $\langle n \rangle$  is comparable to values found in GF liquids for the corresponding  $T$  range (see below). Evidently,  $\langle n \rangle$  increases after cooling (see Fig. 3 *Inset*), where  $\langle n \rangle$  is smaller for  $\Sigma$  GBs than the non- $\Sigma$  GBs,

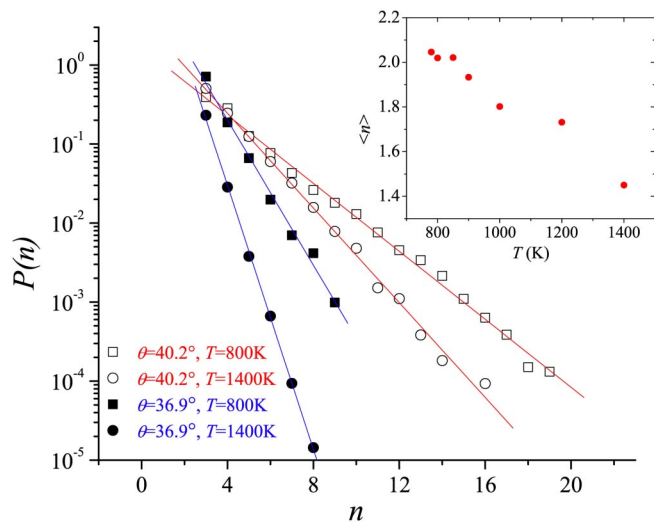


**Fig. 3.** String-length distribution function  $P(n)$  for  $\theta = 36.9^\circ$  boundary ( $\Sigma$  GB) and  $\theta = 40.2^\circ$  boundary (non- $\Sigma$  GB) at 800 and 1,400 K. (Inset) Average string length  $\langle n \rangle$  as a function of  $T$  for the GB, illustrating the growth of the scale of collective atomic motion after cooling. The scale of  $\langle n \rangle$  at a corresponding reduced temperature is similar to that of previous simulation observations on GF liquids (9, 23).

which suggests that atoms in the  $\Sigma$  GBs are less frustrated than those in the more disordered non- $\Sigma$  GBs.

**Comparison of the characteristic temperatures of GB and GF liquids.** We next consider other aspects of the phenomenology of GF liquids that have significance for understanding the transport properties of polycrystalline materials. In particular, glass formation is generally accompanied by thermodynamic changes similar to those observed in rounded thermodynamic transitions, and correspondingly, both of these transitions are characterized by multiple characteristic temperatures (31). We summarize these for GF fluids, and below we determine their analogs for GB dynamics.

The dynamics of GF liquids is characterized by a number of temperatures, which in decreasing order include  $T_A$  (demarking the onset of the cooperative atomic motion), a crossover temperature  $T_c$  (separating high and low  $T$  regimes of glass formation), the glass transition temperature  $T_g$  (below which aging and other nonequilibrium behavior is overtly exhibited), and finally  $T_0$  (characterizing the “end” of the glass-transformation process) (31, 33). To further our analysis, it is natural to consider the analogous characteristic temperatures for the GB MD.  $T_A$  is experimentally defined as the temperature at which the Arrhenius temperature dependence of structural relaxation no longer holds. On the basis of the entropy theory of glass formation (33), the apparent activation energy  $E_a(T)$  below  $T_A$  follows a universal quadratic  $T$  dependence,  $E_a(T)/E_a(T \rightarrow T_A) \approx 1 + C_0(T/T_A - 1)^2$ , where  $C_0$  is a constant. The GB migration mobility data in Fig. 2 Inset fits this relation (SI) well near  $T_A$  (950 K  $< T < 1,400$  K), and we estimate  $T_A$  to equal 1,546 K. To determine the other characteristic temperatures (see SI), we performed a series of simulations to determine the mean-square displacement of atoms  $\langle r^2 \rangle$  within the GBs.

Following Starr et al. (30), we define the Debye–Waller factor (DWF) as the mean-square atomic displacement  $\langle r^2 \rangle$  after a fixed decorrelation time  $t_0$  characterizing the crossover from ballistic to caged atom motion. Fig. 4 shows corresponding data for the GB dynamics where the same criterion is chosen for defining  $t_0$  as described by Starr et al. (30). In GF liquids,  $\langle r^2 \rangle$  at low  $T$  exhibits a well-defined plateau after  $t_0$  that persists up to the structural relaxation time of the fluid  $\tau$  (a time normally many orders of magnitude larger than  $t_0$  for  $T \approx T_g$ ), and the height of this plateau

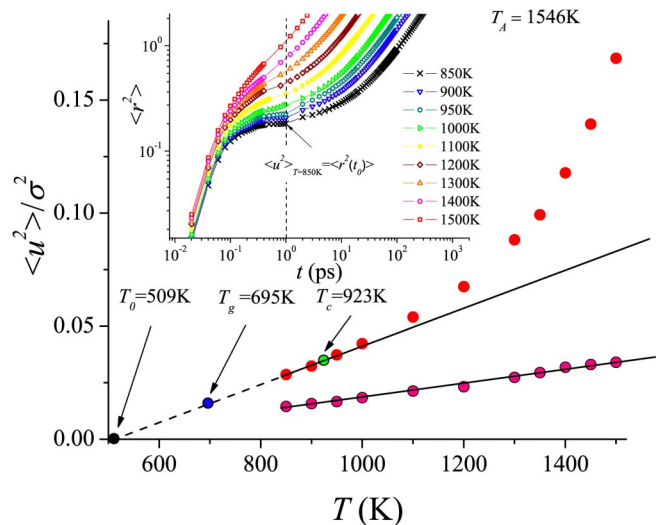


**Fig. 4.** DWF  $\langle u^2 \rangle$  as a function of  $T$  for the GB and crystal. The solid red circles represent the DWF for GB, and the solid pink circles indicate the DWF for the lower grain. We observe that  $\langle u^2 \rangle$  for the GB atomic motion (upper curve) is substantially larger than the scale of atomic motion in the grain (lower curve), with  $\langle u^2 \rangle$  in the grain only obtaining a value comparable to the Lindemann value for temperatures near  $T_m = 1,621$  K (18). The VF temperature  $T_0$ , determined from the  $M(T)$  data in Eq. 2, nearly coincides with the  $T$  at which  $\langle u^2 \rangle$  extrapolates to 0. The temperature  $T_A = 1,546$  K approximates the onset of the supercooling regime and was also determined from the  $M(T)$  data in Fig. 2 (see SI). The crossover temperature  $T_c$  is determined from the GB fluid structural relaxation time (see Fig. 5), and  $T_g$  is estimated by the condition  $\langle u^2 \rangle / \sigma^2 \approx 0.125$ , where  $\sigma$  is the interatomic distance in the crystal, a Lindemann condition for glass formation (33). For the crystal grain,  $\langle u^2 \rangle$  shows linear dependence over the entire  $T$  range. However, for GB,  $\langle u^2 \rangle$  varies nearly linearly with  $T$  (harmonic localization) at low temperatures, but for  $T > T_c$  the harmonic approximation no longer applies. (Inset)  $\langle r^2(t) \rangle$  data from which  $\langle u^2 \rangle \equiv \langle r^2(t_0) \rangle$  was determined. The vertical broken line indicates the inertial decorrelation time,  $t_0$  (30).

defines the size of the “cage” in which particles are transiently localized by their neighbors. In Fig. 4, we observe a progressively flattening of the GB data for  $\langle r^2 \rangle$  at intermediate times that illustrates the progressive caging of atomic motion after cooling in these relatively high-temperature simulations. A well-defined cage (plateau) is apparent only for the lowest temperature simulations indicated. Because  $\langle r^2 \rangle$  is slowly varying with  $t$  in the time interval between  $t_0$  and  $\tau$  in the glass state and because  $\tau$  is on the order of minutes for  $T \approx T_g$ , any experimental estimate of  $\langle r^2 \rangle$  yields a similar value in the glass state over this broad range of time scales. This observation basically explains why dynamic neutron and x-ray scattering measurements of  $\langle r^2 \rangle$  with instrumental time scales on the order of  $10^{-9}$  s are of direct relevance to the physics of glasses. Fig. 4 shows the DWF  $\langle u^2(T) \rangle$  for the GB atomic motion based on the same criterion (i.e.,  $\langle r^2(t_0) \rangle \approx \langle u^2 \rangle$ ) used by Starr et al. (30) for GF fluids. For reasons described below,  $\langle u^2(T) \rangle$  is divided by  $\sigma^2(T)$ , the square of the equilibrium interatomic distance in the crystal. Fig. 4 Inset shows the original GB data from which  $\langle u^2 \rangle$  was determined (the broken line denoting  $t_0$ ).

In addition to the mean particle-displacement scale  $\langle u^2(T) \rangle$  in the caging regime, the distribution function  $G_s(\mathbf{r}, t)$ , for the atomic displacement  $\mathbf{r}(t)$ , also provides valuable information about how much GB atomic motion resembles the dynamics of GF liquids, and this property also allows for the determination of the characteristic temperature  $T_c$  (34, 35). In particular, we calculate the GB self-intermediate scattering function  $F_s(\mathbf{q}, t)$  (35), which is the Fourier transform of  $G_s(\mathbf{r}, t)$ , over a broad temperature range,  $1,050$  K  $\leq T \leq 1,150$  K. Specifically,  $F_s(\mathbf{q}, t)$  is defined as  $F_s(\mathbf{q}, t) = \langle \exp\{-i\mathbf{q}[\mathbf{r}_i(t) - \mathbf{r}_i(0)]\} \rangle$ , where the



had the same magnitude. This sensitivity of  $M$  to the mode of applied stress is difficult to explain in terms of conventional GB migration theories, but this effect is readily understood from our perspective of GB dynamics. In particular, a reexamination of our former simulation results indicates that  $\langle n \rangle$  for 2% tensile and compressive strains at  $T = 800$  K equals 1.63 and 2.13, respectively (*SI*). If one assumes that the apparent activation energy  $Q$  for GB migration can be scaled by  $\langle n \rangle$  [i.e.,  $Q \propto \langle n \rangle E_0$ , where  $E_0$  is the high temperature activation energy (near  $T_A$ )], then the observed change of  $\langle n \rangle$  (and thus  $Q$ ) in tension and compression accounts for the change in magnitude of  $M$ . We suggest that the main origin of this shift in the scale of collective motion  $\langle n \rangle$  derives from a shift of  $T_g$  with deformation, compressive deformation acting similarly to an increase in the hydrostatic pressure, which generally increases  $T_g$ , whereas the extensional deformation has an opposite effect. Temperature and pressure studies will be required to confirm this interpretation of the origin of the deformation-induced changes in  $M$  in terms of the influence of the mode of deformation on cooperative GB atomic motion.

The addition of impurities and nanoscale confinement can also be expected to affect the cooperativity of atomic motions in strained polycrystalline materials, as recently shown in simulations of GF liquids (8, 9). Specifically, if the impurities help relieve packing frustration, then  $\langle n \rangle$  should be greatly attenuated (8) and the  $T$  dependence of  $M$  should be weakened (i.e., the glass formation becomes “stronger”), whereas if the impurities disrupt molecular packing, then the scale of collective motion should become amplified and the  $T$  dependence of  $M$  should be amplified. Large changes in  $M$ , and the resulting properties of polycrystalline materials, are then expected from the application of strains and the presence of impurities through the influence of these effects on the scale of collective motion in the GB region.

## Discussion

We conclude that the atomic dynamics within the GB region of polycrystalline materials and the GB mobility at elevated  $T$

exhibit many features in common with GF liquids. Highly cooperative string-like atom motion in the plane of the GB can greatly affect the average rate of GB motion transverse to the GB plane. This understanding of GB dynamics is expected to shed significant light on the mechanical properties of polycrystals. Indeed, we expect the viscoelastic and highly temperature-dependent properties of the complex GB “fluid” enveloping the crystalline grains to have a large impact on the plastic deformation of these materials. This viewpoint of the polycrystalline materials is contrasted with recent work that attributes the deformational properties of polycrystalline materials to simply the presence of solid crystalline grains within the uncrystallized fluid melt (38, 39). In our view, the uncrystallized material is a “complex fluid” that imparts its own viscoelastic effects on the polycrystalline material. Moreover, the frustrated atoms within the GB region should exhibit a high sensitivity to impurities, pressure, and geometrical confinement as in the case of GF liquids so that we can anticipate significant changes in the plastic deformation properties of polycrystalline materials arising from a modulation of the collective motion in the GB regions through these perturbations. This perspective of polycrystalline materials offers the promise of an increased control of the properties of semicrystalline materials based on further quantification of this phenomenon. Although this conceptual view of polycrystalline materials was intuitively recognized by scientists and engineers involved in the fabrication of iron materials at the beginning of the last century (11), the present work puts this working model of the deformation properties of polycrystalline materials on a sound foundation through direct MD simulation.

**ACKNOWLEDGMENTS.** We thank Robert Riggelman of the University of Wisconsin and Anneke Levelt Sengers of the National Institute of Standards and Technology for helpful comments and questions about the work, and we acknowledge the support of the U.S. Department of Energy (DE-FG02-99ER45797) and the National Institute of Standards and Technology. Useful group discussions were facilitated by the Department Of Energy Office of Basic Energy Sciences Computational Materials Science Network program.

- Ahluwalia R, Lookman T, Saxena A (2003) Elastic deformation of polycrystals. *Phys Rev Lett* 91:055501.
- Sutton AP, Balluffi RW (1995) *Interfaces in Crystalline Materials* (Clarendon, Oxford).
- Gottstein G, Shvindlerman LS (1999) *Grain Boundary Migration in Metals: Thermodynamics, Kinetics, Applications* (CRC Press, Boca Raton, FL).
- Zhu X, Birringer R, Herr U, Gleiter H (1987) *Phys Rev B Condens Matter* 35:9085–9090
- Van Swygenhoven H, Weertman JR (2006) *Mater Today* 9:24–31.
- Rouxel T (2007) Elastic properties and short- to medium-range order in glasses. *J Am Ceram Soc* 90:3019–3039.
- Dzugutov M, Simdyankin SI, Zetterling FHM (2002) Decoupling of diffusion from structural relaxation and spatial heterogeneity in a supercooled simple liquid. *Phys Rev Lett* 89:195701.
- Riggelman RA, Yoshimoto K, Douglas JF, de Pablo JJ (2006) Influence of confinement on the fragility of antiplasticized and pure polymer films. *Phys Rev Lett* 97:045502.
- Riggelman RA, Douglas JF, de Pablo JJ (2007) Tuning polymer melt fragility with antiplasticizer additives. *J Chem Phys* 126:234903.
- Riggelman RA, Douglas JF, De Pablo JJ (2007) Characterization of the potential energy landscape of an antiplasticized polymer. *Phys Rev E Stat Nonlin Soft Matter Phys* 76:011504.
- Rosenhain W, Ewen D (1913) The intercrystalline cohesion of metals. *J Inst Met* 10:119–149.
- Ashby MF (1972) Boundary defects, and atomistic aspects of boundary sliding and diffusional creep. *Surf Sci* 31:498–542.
- Keblinski P, Phillipot SR, Wolf D, Gleiter H (1996) Thermodynamic criterion for the stability of amorphous intergranular films in covalent materials. *Phys Rev Lett* 77:2965–2968.
- Wolf D (2001) High-temperature structure and properties of grain boundaries: long-range vs. short-range structural effects. *Curr Opin Solid State Mater Sci* 5:435–443.
- Read WT, Shockley W (1950) Dislocation models of crystal grain boundaries. *Phys Rev* 78:275–289.
- Sutton AP, Vitek V (1983) On the structure of tilt grain-boundaries in cubic metals. 1. Symmetrical tilt boundaries. *Philos Trans R Soc London Ser A* 309:1–68.
- Randle V, Engler O (2000) *Introduction to Texture Analysis: Macrotexture, Microtexture and Orientation Mapping* (Gordon & Breach, Amsterdam, The Netherlands).
- Zhang H, Srolovitz DJ, Warren J, Douglas JF (2006) Characterization of atomic motions governing grain boundary migration. *Phys Rev B Condens Matter* 74:115404.
- Hoover WG, Holian BL (1996) Kinetic moments method for the canonical ensemble distribution. *Phys Lett A* 211:253–257.
- Voter AF, Chen SP (1987) Accurate interatomic potentials for Ni, Al and Ni3Al. *Mater Res Soc Symp Proc* 82:175–180.
- Zhang H, Mendelev MI, Srolovitz DJ (2004) Computer simulation of the elastically driven migration of a flat grain boundary. *Acta Mater* 52:2569–2576.
- Zhang H, Srolovitz DJ, Douglas JF, Warren J (2007) Atomic motion during the migration of general [001] tilt grain boundaries in Ni. *Acta Mater* 55:4527–4533.
- Donati C, et al. (1998) Stringlike cooperative motion in a supercooled liquid. *Phys Rev Lett* 80:2338–2341.
- Donati C, Glotzer SC, Poole PH, Kob W, Plimpton SJ (1999) Spatial correlations of mobility and immobility in a glass-forming Lennard–Jones liquid. *Phys Rev E Stat Phys Plasmas Fluids Relat Interdiscip Top* 60:3107–3119.
- Marcus AH, Schofield J, Rice SA (1999) Experimental observations of non-Gaussian behavior and stringlike cooperative dynamics in concentrated quasi-two-dimensional colloidal liquids. *Phys Rev E Stat Phys Plasmas Fluids Relat Interdiscip Top* 60:5725–5736.
- Weeks ER, Crocker JC, Levitt AC, Schofield A, Weitz DA (2000) Three-dimensional direct imaging of structural relaxation near the colloidal glass transition. *Science* 287:627–631.
- Adam G, Gibbs JH (1965) On temperature dependence of cooperative relaxation properties in glass-forming liquids. *J Chem Phys* 43:139–146.
- Porter DA, Easterling KE (1993) *Phase Transformations in Metals and Alloys* (Chapman & Hall, New York).
- Angell CA (1995) Formation of glasses from liquids and biopolymers. *Science* 267:1924–1935.
- Starr FW, Sastry S, Douglas JF, Glotzer SC (2002) What do we learn from the local geometry of glass-forming liquids? *Phys Rev Lett* 89:125501.
- Douglas JF, Dudowicz J, Freed KF (2006) Does equilibrium polymerization describe the dynamic heterogeneity of glass-forming liquids? *J Chem Phys* 125:144907.
- Keys AS, Abate AR, Glotzer SC, Durian DJ (2007) Measurement of growing dynamical length scales and prediction of the jamming transition in a granular material. *Nat Phys* 3:260–264.
- Dudowicz J, Freed KF, Douglas JF (2007) Generalized entropy theory of polymer glass formation. *Adv Chem Phys* 137:125–223.
- Kob W, Andersen HC (1994) Scaling behavior in the beta-relaxation regime of a supercooled Lennard–Jones mixture. *Phys Rev Lett* 73:1376–1379.
- Hansen JP, McDonald IR (1986) *Theory of Simple Liquids* (Academic, New York).
- Larini L, Ottochian A, De Michele C, Leporini D (2008) Universal scaling between structural relaxation and vibrational dynamics in glass-forming liquids and polymers. *Nat Phys* 4:42–45.
- Wang WH (2005) Elastic moduli and behaviors of metallic glasses. *J Non-Cryst Solids* 351:1481–1485.
- Gourlay CM, Dahle AK (2007) Dilatant shear bands in solidifying metals. *Nature* 445:70–73.
- Martin CL, Braccini M, Suery M (2002) Rheological behavior of the mushy zone at small strains. *Mater Sci Eng A Struct Mater* 325:292–301.